ISSN 1063-7761, Journal of Experimental and Theoretical Physics, 2017, Vol. 124, No. 4, pp. 584–591. © Pleiades Publishing, Inc., 2017.
Original Russian Text ©A.N. Shaimanov, K.M. Khabarov, A.M. Merzlikin, I.V. Bykov, A.V. Baryshev, 2017, published in Zhurnal Eksperimental'noi i Teoreticheskoi Fiziki, 2017, Vol. 151, No. 4, pp. 686–694.

SOLIDS AND LIQUIDS

Plasmon Resonances in a Two-Dimensional Lattice of Metal Particles in a Dielectric Layer: Structural and Polarization Properties

A. N. Shaimanov[a,b]*, K. M. Khabarov[a,c], A. M. Merzlikin[a,c,e], I. V. Bykov[a,e,f], and A. V. Baryshev[a,c,d]**

[a] *All-Russia Research Institute of Automatics, ul. Sushchevskaya 22, Moscow, 127055 Russia*

[b] *Moscow State University, Moscow, 119991 Russia*

[c] *Moscow Institute of Physics and Technology, Dolgoprudnyi, Moscow oblast, 141700 Russia*

[d] *Ioffe Physico-Technical Institute, Russian Academy of Sciences, Polytekhnicheskaya ul. 26, St. Petersburg, 194021 Russia*

[e] *Institute for Theoretical and Applied Electromagnetics, Russian Academy of Sciences, Izhorskaya ul. 13, Moscow, 125412 Russia*

[f] *Bauman Moscow State Technical University, Vtoraya Baumanskaya ul. 5, Moscow, 105005 Russia*

* *e-mail: shaymanov@inbox.ru*

** *e-mail: baryshev@vniia.ru*

Received August 16, 2016

Abstract—The results of experimental and theoretical investigation of planar two-dimensional (2D) samples of plasmon structures are presented. The samples represent a 2D lattice of gold nanoparticles embedded in a thin dielectric layer and are studied by atomic force microscopy (AFM) and optical methods. Absorption bands associated with the excitation of various surface plasmon resonances (SPR) are interpreted. It is found that the choice of the mutual orientation of the polarization plane and the edge of the unit cell of the 2D lattice determines the spectral position of the lattice surface plasmon resonance (LSPR) related to the lattice period. It is shown that the interaction of *p*- and *s*-polarized light with a 2D lattice of nanoparticles is described by the dipole–dipole interaction between nanoparticles embedded in a medium with effective permittivity. Analysis of the spectra of ellipsometric parameters allows one to determine the amplitude and phase anisotropy of transmission, which is a consequence of the imperfection of the 2D lattice of samples.

DOI: 10.1134/S1063776117030165

Nanoparticles of noble metals attract special attention due to the fact that disordered and periodic structures based on these particles exhibit localized surface plasmon resonances (SPRs) [1, 2]. It is known that the localization of the electric field and a significant increase in its amplitude on the surface of nanoparticles are attractive for photovoltaics [3, 4], amplification of magneto-optical [5–7] and nonlinear optical effects [8, 9], detection of biological substances [10, 11], and design of surface plasmon lasers [12].

The optical properties of plasmon structures (based on nanoparticles) depend on the shape and the material of an isolated nanoparticle, on the permittivity of the medium surrounding a nanoparticle [2, 13], on the distance between nanoparticles and their arrangement [14, 15], as well as on the polarization of the incident radiation. The transmission spectra of nanoparticle-based periodic structures exhibit features related to the lattice SPR (LSPR) [2, 16–20]. The study of the LSPR is of practical interest because of the high sensitivity of the resonance to the change in the local environment of the structure: small variations in dielectric permittivity may lead to a significant change in the spectral position of the LSPR [21], which can be used in optical biosensors [22]. It was shown that the choice of the period of a 2D lattice of plasmon nanoparticles allows one to control the spectral position of the LSPR in structures based on magneto-optical materials and strongly enhance their response at LSPR frequencies [23, 24].

In spite of a rather extensive investigation of plasmon 2D structures, the study of the LSPR in structures representing a 2D lattice of metal nanoparticles in a thin dielectric layer was addressed only in a few papers [8, 23]. In our study, we carry out a detailed experimental and theoretical analysis of these structures with different periods of the 2D lattice. The transmission spectra of the samples exhibit absorption

bands associated with the excitation of the SPR and the LSPR. The study of samples by atomic force microscopy (AFM) revealed structural features of these resonances, while the spectra of ellipsometric parameters allowed one to determine the structural anisotropy of the samples. The results of experimental and theoretical investigations are in good agreement.

Experimental samples based on gold and bismuth-substituted yttrium iron garnet (Au–Bi: YIG) were fabricated by electron-beam deposition, electron lithography, and ion etching. At the first stage, we produced a square 2D lattice of gold nanodisks from a 30-nm-thick gold film on a quartz substrate; the lattice parameters D for three samples were $D_1 \approx 200$ nm, $D_2 \approx 300$ nm, and $D_3 \approx 400$ nm. First, we heated the gold nanodisk lattice to the crystallization temperature of the Bi : YIG compound (750°C). Heating is a necessary step toward the stabilization of the shape of nanoparticles for subsequent deposition and annealing of the Bi : YIG film. The deposited Bi : YIG film had a thickness of $d \approx 100$ nm and a polycrystalline structure of $Bi_1Y_2Fe_5O_{12}$. Thus, the samples represented a square 2D lattice of gold nanoparticles placed on a quartz substrate and coated with a Bi : YIG film. The geometric dimensions of a sample were 4×4 mm^2.

A top view and a surface profile of one of the samples ($D_2 \approx 300$ nm) are shown in Figs. 1a–1c. On the basis of the results of AFM studies, we found that the surface of the samples has a sinusoidal profile (see the section of an AFM image in Fig. 1c). It seems that the gold nanodisks had been fused due to heating and took a spheroidal form. We analyzed the parameters of the 2D lattice along x and y axes, D_x and D_y, for all the samples, as is shown in Figs. 1a and 1c. A specific feature of mapping by AFM is the fact that, in scanning the surface, there exist fast and slow axes. Therefore, there may be small contractions and extensions of images due to the sample drift. For example, for the second sample ($D_2 \approx 300$ nm), the lattice period along the fast scanning axis is $D_{2x} = 300$ nm and along the slow axis, $D_{2y} = 304$ nm. To determine the parameters D_x and D_y without the drift effect, we carried out more accurate measurements for the second sample after double calibration of the microscope when the fast scanning axis coincides with either x or y axis. In this case, we scanned two areas with a size of 50×50 μm^2.

According to the results of processing AFM images, the periods in one of the scanning areas were $D_{2x} = 307.5 \pm 1.4$ nm and $D_{2y} = 306.2 \pm .5$ nm, while in the other area, $D_{2x} = 304.3 \pm 1.9$ nm and $D_{2y} = 305.8 \pm 0.9$ nm. The data obtained by AFM allow one to verify that the lattice is square in the areas considered. However, the lattice structure over the entire area of a sample was nonideal, i.e., there were period fluctuations along both the x and y axis.

The transmission spectra and the ellipsometric parameters ψ and Δ were measured by an ellipsometer (Ellipse 1891 SAG) in the wavelength range of 350–1050 nm. The measurements were carried out for $\mathbf{E}_x$-, $\mathbf{E}_y$-, and $\mathbf{E}_{45°}$-polarized light in the xy plane (see Fig. 1a). The samples were illuminated by a parallel beam of polarized light in the geometry of normal and oblique incidence; the exposed area did not exceed the size of a sample (4×4 mm^2) and was about 1 mm^2. Below, we will discuss that optical spectra allow one to determine the average period of the lattice of the samples due to the dependence of the spectral position of the LSPR on the lattice period.

In the case of a plasmon square 2D lattice fabricated on a substrate, we show that the spectral position of the LSPR is determined by the lattice period and the refractive index of the substrate [19]. It is also known that, for structures consisting of asymmetric nanoparticles or dimers (two plasmon nanoparticles side by side), the position of an SPR in the optical spectra depends on the polarization of incident radiation [14, 25]. Therefore, the appearance of plasmon resonances in the polarization spectra of plasmon 2D structures allows one to determine the symmetry of both an isolated scatterer and the entire structure.

Figure 2a demonstrates the experimental transmission spectra of three samples in normal incidence geometry ($\theta = 0$). One can see that, for an incident wave with $\mathbf{E}_x$ and $\mathbf{E}_y$ polarizations, the transmission spectra exhibit two main features (indicated by arrows): short-wavelength (heavy arrows) and long-wavelength (thin arrows) bands. As the lattice period D increases from 200 to 400 nm, the short-wavelength band is shifted in the range of $\lambda = 550–600$ nm, while the shift of the long-wavelength band is proportional to the growth of D in the range of $\lambda = 690–820$ nm. It is important that the spectral position of the short-wavelength band does not depend on the polarization, while the long-wavelength bands for $\mathbf{E}_x$ and $\mathbf{E}_y$ polarizations are shifted with respect to each other in all the samples.

The short-wavelength band in Fig. 2a is attributed to the excitation of SPR of individual nanoparticles. A condition under which this resonance is excited is described by the Mie theory and is determined by the following expression for a spherical nanoparticle [26]:

$$\mathrm{Re}\{\varepsilon_{Au}(\lambda)\} = -2\varepsilon_{Bi:YIG}(\lambda), \quad (1)$$

where ε_{Au} and $\varepsilon_{Bi:YIG}$ are the permittivities of Au and Bi : YIG. Indeed, for example, for a sample with $D_1 \approx 200$ nm, $\mathrm{Re}\{\varepsilon_{Au}(\lambda = 587\ \mathrm{nm})\} \approx -10.5$ [27] and $\varepsilon_{Bi:YIG}(\lambda = 597\ \mathrm{nm}) \approx 10.5$.[1] Note that the difference in the spectral positions of the SPR band in the samples can be attributed to the unequal size of nanoparticles for different lattice periods, as well as to the finiteness

[1] The optical constant of thin Bi : YIG films were determined by a J.A. Woollman Co. ellipsometer.

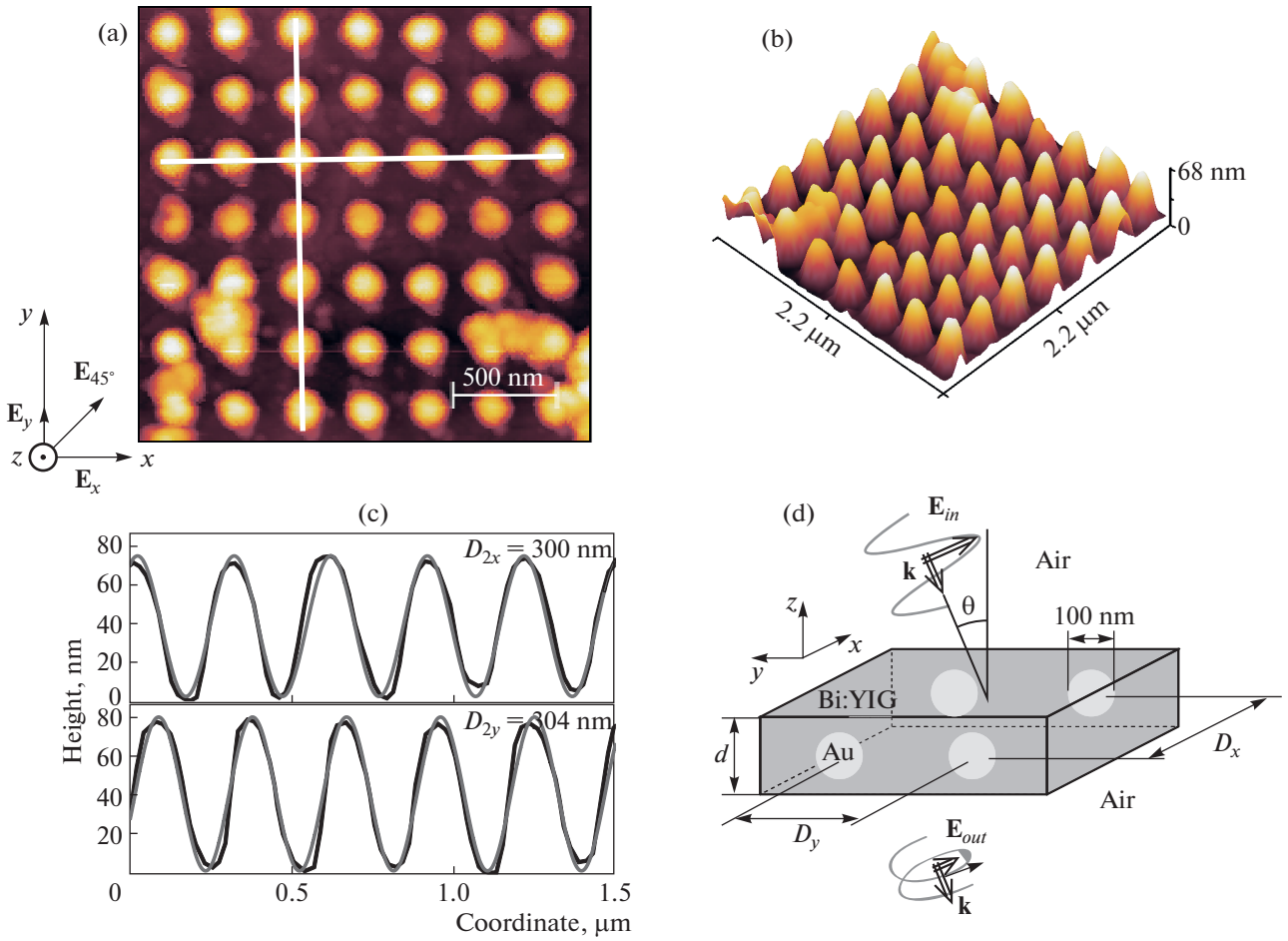

Fig. 1. (a, b) AFM images of a sample with period $D_2 \approx 300$ nm. (c) Cross section of the surface in Fig. 1a and its approximation by a sinusoidal function. (d) Model for numerical simulation.

of the thickness of the Bi : YIG film, in which the gold particles feel not only the surrounding Bi : YIG but also the Bi : YIG/air interface.

According to [1, 20], the spectral position of the long-wavelength band is determined by the dipole–dipole interaction of nanoparticles when the lattice period is the defining parameter. Indeed, it turns out that the spectral position of the long-wavelength band in the samples analyzed in normal incidence geometry is well described by the diffraction condition [23]

$$m\lambda = n_{\text{eff}} D, \tag{2}$$

where $m = 1$, D is the lattice period and n_{eff} is the effective refractive index calculated by the Maxwell–Garnett (MG) formula for spherical gold particles in a Bi : YIG layer (see footnote 1),

$$n_{\text{eff}}^2 = n_{\text{Bi:YIG}}^2 \left[1 - \frac{3V(n_{\text{Bi:YIG}}^2 - \text{Re}\,\varepsilon_{\text{Au}})}{2n_{\text{Bi:YIG}}^2 + \text{Re}\,\varepsilon_{\text{Au}} + V(n_{\text{Bi:YIG}}^2 - \text{Re}\,\varepsilon_{\text{Au}})}\right], \tag{3}$$

where V is the volume fraction of Au and $n_{\text{Bi:YIG}}$ is the refractive index of Bi : YIG (see footnote 1).

Note that the diffraction condition (2) for $m = 2$ well describes the spectral position of the absorption band of the LSPR ($\lambda = 650$ nm) for the third sample ($D_3 = 400$ nm) with $n_{\text{eff}} = 3.17$ (see Fig. 2a). Notice that this feature also manifests itself in the calculated spectra (see Fig. 2b). Namely, the absorption band near $\lambda = 630$ nm for the third sample has a complex shape due to the spectral intersection between the absorption band due to the Mie resonance of an isolated particle and the LSRP band described by condition (2) for $m = 2$.

Apparently, the cross section of an isolated nanoparticle has a circular shape because the spectral position of the short-wavelength band does not

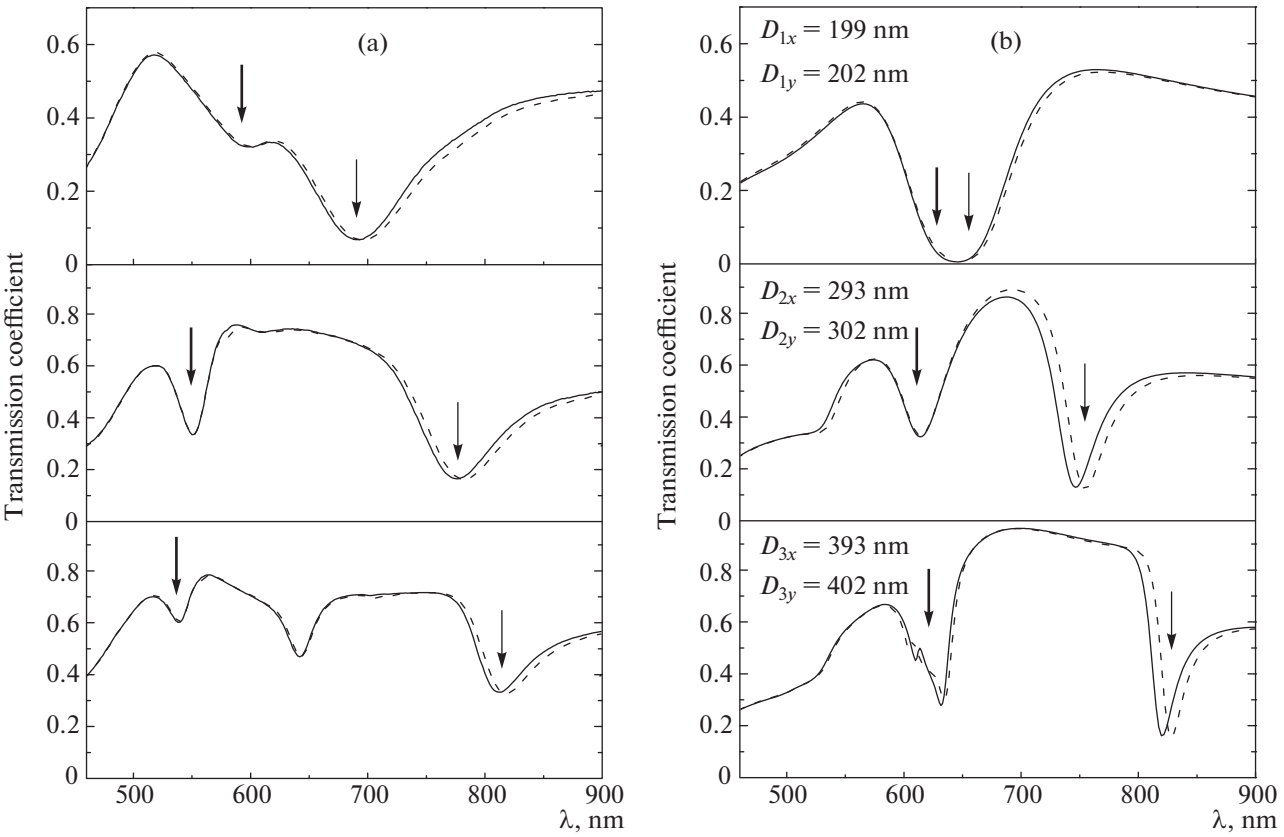

Fig. 2. (a) Experimental and (b) theoretical transmission spectra as a function of wavelength for structures with periods D_1, D_2, and D_3 under normal incidence of light on the samples when the electric field is directed along the x (solid lines) and y (dashed lines) axes.

depend on the polarization of the incident wave. Conversely, the difference in the spectral positions of long-wavelength bands for $\mathbf{E}_x$- and $\mathbf{E}_y$-polarized light gives evidence of the structural anisotropy of the samples. Using the COMSOL program, we calculated the transmission spectra of structures with a rectangular lattice of spherical nanoparticles embedded in a 150-nm-thick Bi : YIG layer with periods D_x and D_y along the x and y axes, respectively (see Fig. 1d), such that the calculated and experimental spectral positions of the LSPR bands for $\mathbf{E}_x$- and $\mathbf{E}_y$-polarized light coincide (Fig. 2b). The results of the analysis of experimental and calculated spectra for periods D_x and D_y are presented in the table.

Thus, the positions of the minima of the absorption bands in the polarization transmission spectra of the structures differ by $\Delta\lambda(D_1) = 3$ nm, $\Delta\lambda(D_2) = 9$ nm, and $\Delta\lambda(D_3) = 9$ nm. Assuming that an isolated scatterer in all three samples is symmetric with respect to the x and y axes, we can attribute the differences $\Delta\lambda$ to the difference in the lattice period along the x and y axes. Note that the values of D recovered from the experimental and calculated optical spectra by expression (1) do not quite coincide with the results of AFM mapping. The latter fact can be associated with the difference in the size of the analysis area: 100×100 μm^2 in the case of AFM and 1×1 mm^2 in the case of optical investigations, when the results are averaged over a large area of the sample.

Note also that we found a significant difference between the spectral bandwidths of SPR and LSPR in the experimental spectra. The analysis of the experimental and calculated spectra by Gaussian curve fitting carried out for $D \approx 300$ nm has shown that $\Delta\lambda_{SPR} \approx 25$ nm and $\Delta\lambda_{LSPR} \approx 75$ nm in the experiment and $\Delta\lambda_{SPR} \approx \Delta\lambda_{LSPR} \approx 45$ nm in calculation (see Fig. 2). The expansion of the LSPR band of experimental structures is most likely attributed to the fluctuation of the crystal lattice period and the deviation of the profile of the Bi : YIG/air interface from the sinusoidal shape.

Consider the transmission spectra of the second sample ($D_2 \approx 300$ nm) measured for obliquely incident light (Fig. 3). One can see that, for p-polarized light, the spectral position of the LSPR changes little, unlike the case of s-polarized light, where the LSPR is shifted to greater wavelengths with increasing angle of incidence. Using the COMSOL program, we calculated the transmission spectra for s- and p-polarized light.

Effective refractive indices of experimental samples by the results of analysis of calculated and experimental transmission spectra

Period D_j by AFM	Calculated period D_i	МГ* $n_{\text{eff}}(\lambda_{\text{exp}})$	Calculation $n_{\text{eff}} = \lambda_{\text{mod}}/D_i$	Experiment $n_{\text{eff}} = \lambda_{\text{exp}}/D_i$
$D_1 = 192.0 \pm 2.7$ nm	$D_{1x} = 199$ nm	3.50	3.31	3.61 ± 0.05
	$D_{1y} = 202$ nm	3.40	3.27	
$D_2 = 305.9 \pm 2.7$ nm	$D_{2x} = 293$ nm	2.47	2.55	2.541 ± 0.03
	$D_{2y} = 302$ nm	2.46	2.50	
$D_3 = 383.0 \pm 2.7$ nm	$D_{3x} = 393$ nm	2.31	2.08	2.121 ± 0.02
	$D_{3y} = 402$ nm	2.30	2.05	

λ_{mod} and λ_{exp} are the minima of the LSPR absorption bands of calculated and experimental transmission spectra; * calculation by the MG formula (3) is performed for the unit cell of a square lattice with periods D_x and D_y and the refractive indices of materials at wavelength λ_{exp}. (Notice that, for the structure with period $D \approx 400$ nm (see Fig. 2), the transmission spectrum has a minimum of the LSPR absorption band calculated by formula (2) with $m = 2$ and $n_{\text{eff}} = 3.17$.)

To explain the difference between the transmission spectra for *s*- and *p*-polarized light, we represent a nanoparticle as a radiating electric dipole. We begin the analysis of the spectra with *s*-polarization (Fig. 4a). In this case, the interaction between dipoles occurs along $\mathbf{k}_x$ (the projection of the wave vector of the incident wave onto the *x* axis). For *s*-polarized light, adjacent dipoles radiate with a phase shift due to the path difference $D\sin\theta$, which leads to a shift in the spectral position of the LSPR band with variation in

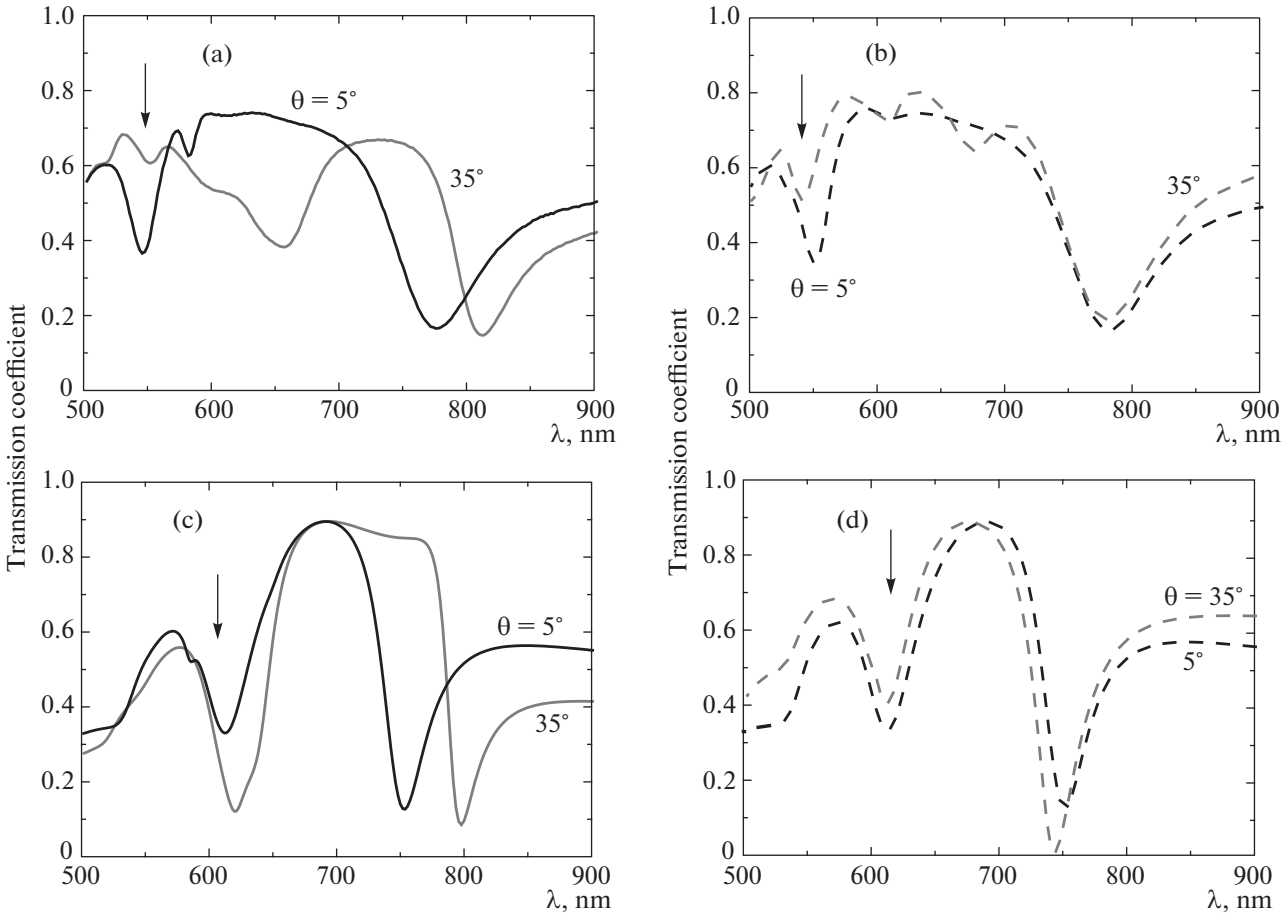

Fig. 3. (a, b) Experimental and (c, d) calculated transmission spectra for a structure with period D_2 for *s* polarization (solid lines) and *p* polarization (dashed lines) for different angles of incidence θ on the sample.

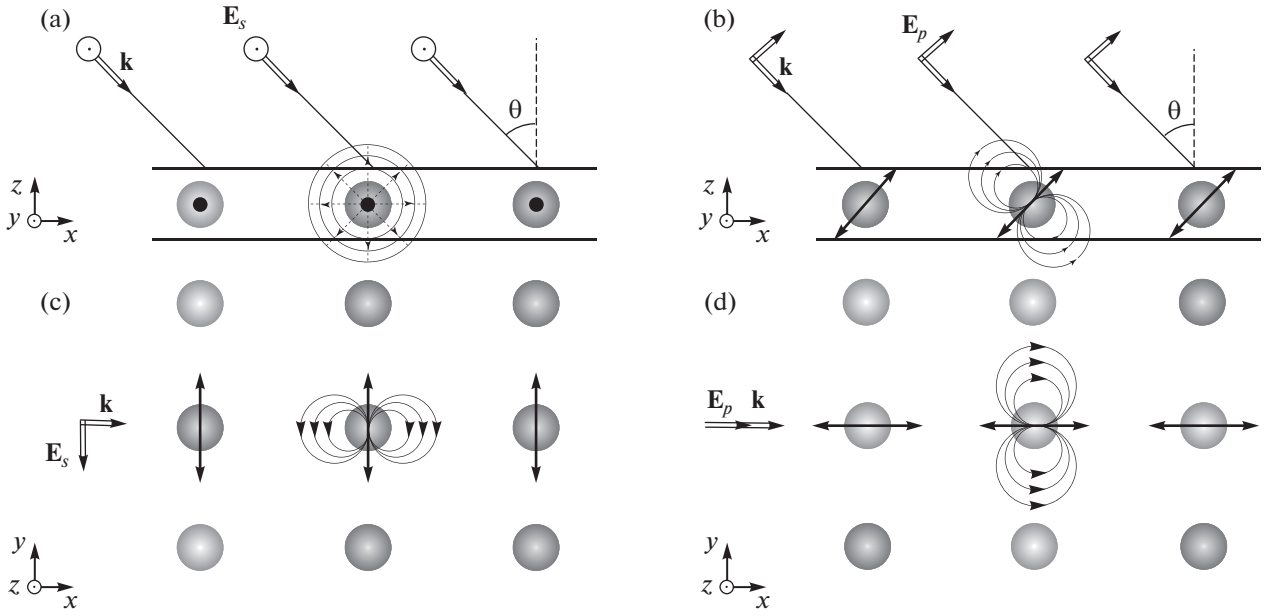

Fig. 4. Illustration to the explanation of the spectral shift of the LSPR in the case of oblique incidence of an (a, c) *s*-polarized and (b, d) *p*-polarized light on the structure; (a, b) side view and (c, d) top view.

the angle of incidence θ (see Fig. 3a). In the case of a *p*-polarized incident wave (Fig. 4b), dipoles interact along the *y* axis, and their interaction along the *x* axis is small. This accounts for the weak dependence of the spectral position of the long-wavelength minimum on the angle of incidence θ.

We have found that the intensity and the spectral position of the SPR band related to the Mie resonance (which is indicated by an arrow in Fig. 3) vary for oblique incidence. As is known, in the case of asymmetric particles, the Mie resonance is split [13]. In our case, we used a spherical nanoparticle surrounded by a dielectric layer of finite thickness as a model for calculating the transmission spectra (see Fig. 1d). Apparently, even in this model, the effective dielectric environment of nanoparticles depends on the orientation of the electric field of the incident wave in view of the finite thickness of the dielectric layer.

Let us analyze the spectra presented in Fig. 3a; namely, consider how the spectral position of the LSPR for *s*-polarized light depends on the angle of incidence. According to (1), the first diffraction order propagates along the lattice of nanoparticles. In normal incidence geometry, adjacent nanoparticles radiate with a phase shift due to the path difference *BC* (Fig. 5a). Since the collective interaction of nanoparticles occurs along the *x* axis, the projection of the path difference *BC* onto this axis is responsible for the spectral shift of the LSPR:

$$AB = BC\sin\varphi = \frac{D\sin^2\theta}{n_{\text{eff}}}, \qquad (4)$$

where the angle φ is determined from the refraction law $n_{\text{eff}}\sin\varphi = n_{\text{air}}\sin\theta$, where n_{eff} is the effective refractive index calculated by expression (3).

Thus, the spectral position of the LSPR band is described by the following expression:

$$\lambda = \lambda_{\theta=0} + \frac{D\sin^2\theta}{n_{\text{eff}}}, \qquad (5)$$

where $\lambda_{\theta=0}$ is the position of the LSPR for $\theta = 0$. Figure 5b demonstrates the calculated and experimental wavelengths of LSPR as a function of the angle of incidence θ. Figure 5 shows that the calculated functions are well approximated by the dependence (5) for samples with D_1 and D_2, while, in the case of a sample with D_3, there is a discrepancy. The latter is attributed to the fact that the value of n_{eff} calculated by expression (3) is greater compared with the values of n_{eff} obtained from the analysis of experimental and calculated transmission spectra (see the table).

It is known that the amplitude and phase anisotropy of transmission of periodic structures can be analyzed by means of ellipsometry [28]. Indeed, these studies provide the best means for determining the structural features of samples associated with the imperfection of their crystal lattice. As shown above, one can distinguish two features in the spectra of the structures investigated: the SPR and LSPR absorption bands. Figure 6a demonstrates the experimental spectra of the ellipsometric parameters ψ and Δ for linearly polarized light with $\mathbf{E}_{45^\circ}$-polarization. One can see that both parameters vary significantly in the region of LSPR compared with other spectral ranges, including the SPR region.

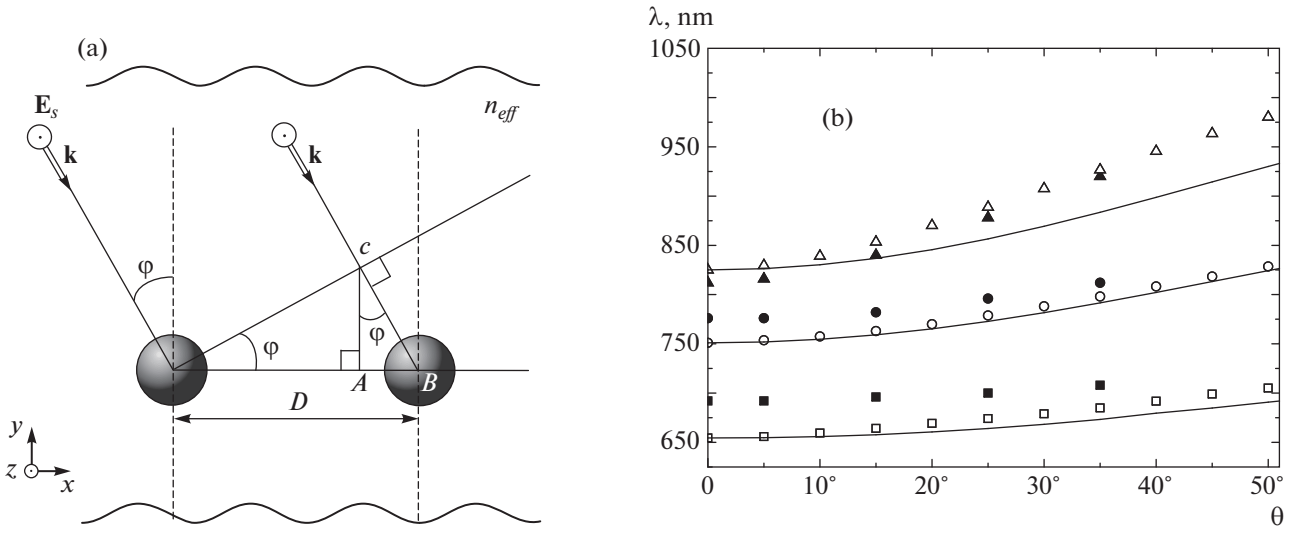

Fig. 5. (a) Illustration to the explanation of the spectral shift of the LSPR in the case of oblique incidence of *s*-polarized light. (b) Spectral position of the LSPR as a function of the angle of incidence θ for structures with D_1 (squares), D_2 (circles), and D_3 (triangles); (open symbols) calculated and (closed symbols) experimental results; (solid lines) spectral position of the LSPR according to (5).

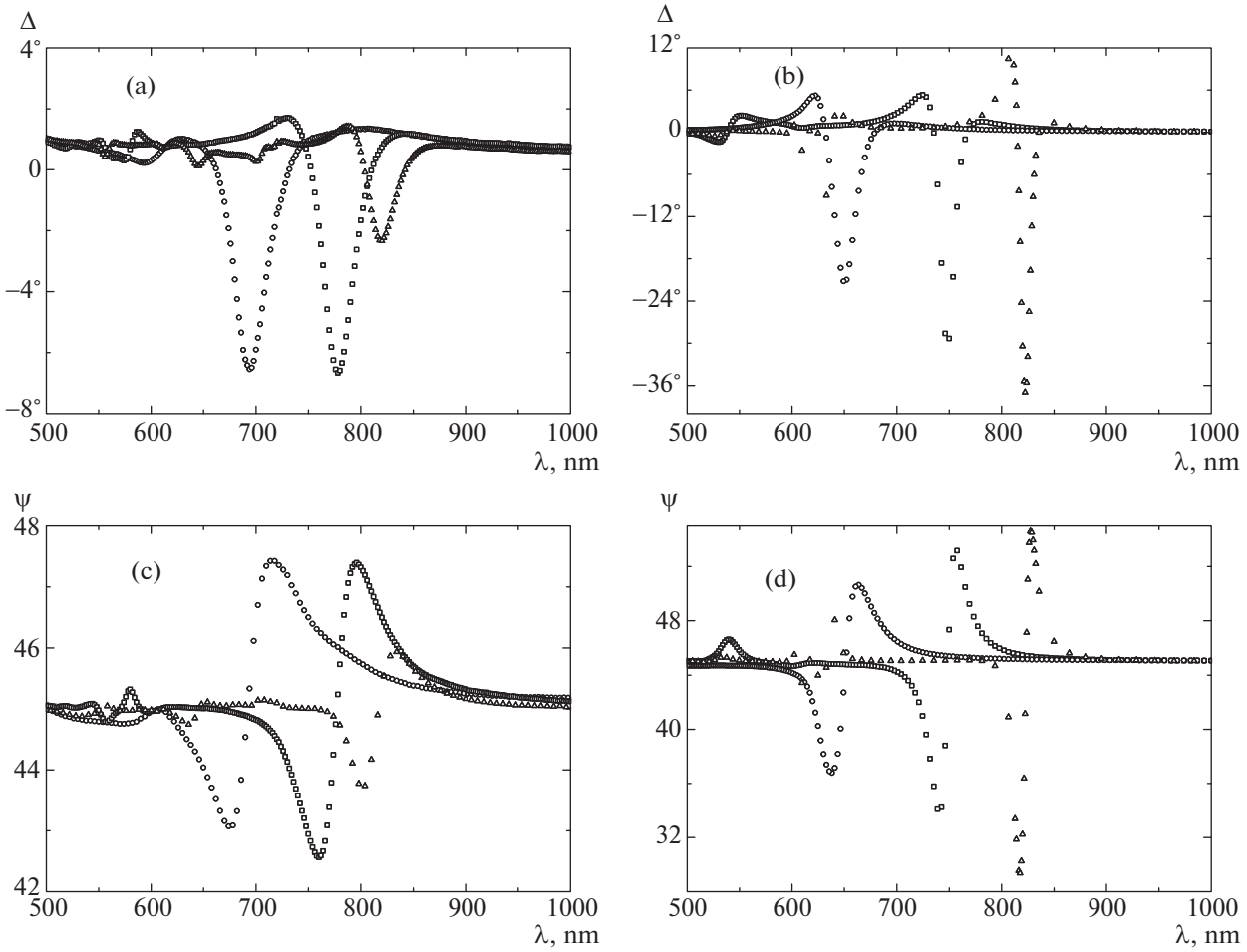

Fig. 6. (a) Experimental and (b) calculated spectra of ψ and Δ under normal incidence for samples with D_1 (circles), D_2 (squares), and D_3 (triangles).

Figure 6b demonstrates the spectra of ψ and Δ for structures with calculated periods from the table. Let us carry out a comparative analysis of the experimental and calculated spectra. We can see a qualitative similarity between the spectra; however, the experimental ψ and Δ have smaller values. Apparently, this is associated with the fact that the samples exhibit lattice period fluctuations over the sample area (according to the AFM data), while the calculations were made for a model with an ideal rectangular lattice.

To summarize, we have investigated the structural features and interpreted the optical properties of plasmon 2D structures (a 2D lattice of metal particles in a dielectric layer). We have found absorption bands in the transmission spectra at the plasmon resonance frequency both for an isolated particle and a 2D ensemble of particles. The analysis of the polarization transmission spectra has shown that the 2D lattice of the samples is rectangular. At the plasmon resonance frequencies, the spectra of ellipsometric parameters exhibit features related to the amplitude and phase anisotropy of transmission due to the imperfection of the structure of the samples. Investigations have shown that the spectra of ellipsometric parameters allow one to determine with high accuracy both the symmetry of an individual scatterer and the imperfection of the 2D lattice. We have demonstrated a good agreement between the experimental and calculated spectra.

The results of investigation of the polarization transmission spectra in oblique incidence geometry have allowed us to demonstrate that the lattice surface plasmon resonance is attributed to the dipole–dipole interaction of particles in a 2D lattice. We have found that the mutual orientation between the lattice of scatterers and the polarization of the incident radiation determines the spectral position of the lattice surface plasmon resonance.

ACKNOWLEDGMENTS

We are grateful to T.V. Murzina, I.A. Kolmychek, and I.A. Ryzhikov for useful discussions and help in carrying out experiments.

This work was supported by the Foundation for Perspective Research, contract no. 7/004/2013-2018 of December 23, 2013.

REFERENCES

1. H. Raether, *Surface Plasmons on Smooth and Rough Surfaces and on Grating* (Springer, Berlin, 1988).
2. S. A. Maier, *Plasmonics: Fundamentals and Applications* (Springer, Berlin, 2007).
3. K. D. G. Imalka Jayawardena, L. J. Rozanski, C. A. Mills, et al., Nanoscale **5**, 8411 (2013).
4. D. M. O'Carroll, Ch. E. Petoukhoff, J. Kohl, et al., Polym. Chem. **4**, 5181 (2013).
5. L. E. Kreilkamp, V. I. Belotelov, J. Y. Chin, et al., Phys. Rev. X **3**, 041019 (2013).
6. V. L. Krutyanskiy, I. A. Kolmychek, E. A. Gan'shina, et al., Phys. Rev. B **87**, 035116 (2013).
7. I. A. Kolmychek, A. N. Shaimanov, A. V. Baryshev, and T. V. Murzina, JETP Lett. **102**, 46 (2015).
8. E. M. Kim, S. S. Elovikov, T. V. Murzina, et al., Phys. Rev. Lett. **95**, 227402 (2005).
9. I. A. Kolmychek, T. V. Murzina, S. Fourier, et al., Solid State Phenom. 152-—153, 508 (2009).
10. S. Chen, M. Svedendahl, M. Kiill, et al., Nanotechnology **20**, 434015 (2009).
11. A. V. Kabashin and P. I. Nikitin, Opt. Commun. **150**, 5 (1998).
12. P. Berini and I. de Leon, Nat. Photon. **6**, 16 (2012).
13. C. L. Nehl and J. H. Hafner, J. Mater. Chem. **18**, 2415 (2008).
14. P. K. Jain and M. A. El-Sayed, Chem. Phys. Lett. **487**, 153 (2010).
15. M. Ranjan, M. Bhatnagar, and S. Mukherjee, J. Appl. Phys. **117**, 103106 (2015).
16. A. I. Väkeväinen, R. J. Moerland, and H. T. Rekola, Nano Lett. **14**, 1721 (2014).
17. V. A. Markel, J. Mod. Opt. **40**, 2281 (1993).
18. S. Zou, N. Janel, and G. C. Schatz, J. Chem. Phys. **120**, 10871 (2004).
19. Y. Chu, E. Schonbrun, T. Yang, and K. B. Crozier, Appl. Phys. Lett. **93**, 181108 (2008).
20. B. Lamprecht, G. Schider, R. T. Lechner, et al., Phys. Rev. Lett. **84**, 4721 (2000).
21. S. Zou and G. C. Schatz, Chem. Phys. Lett. **403**, 62 (2005).
22. A. J. Haes and R. P. van Duyne, J. Am. Chem. Soc. **124**, 10596 (2002).
23. A. Baryshev and A. Merzlikin, J. Opt. Soc. Am. B **33**, 1399 (2016).
24. G. Armelles, A. Cebollada, A. García-Martín, et al., Adv. Opt. Mater. **1**, 10 (2013).
25. H. Husu, J. Mäakitalo, J. Laukkanen, et al., Opt. Express **18**, 16601 (2010).
26. G. Mie, Ann. Phys. (Leipzig) **25**, 377 (1908).
27. K. M. McPeak, S. V. Jayanti, S. J. P. Kresset, et al., ACS Photon. **2**, 326 (2015).
28. H. Fujiwara, *Spectroscopy Ellipsometry: Principles and Applications* (Wiley, New York, 2007).

Translated by I. Nikitin